UCRL-JRNL-230636

LAWRENCE
LIVERMORE
NATIONAL
LABORATORY

Electron Density Measurements in the National Spherical Torus Experiment Detached Divertor Region Using Stark Broadening of Deuterium Infrared Paschen Emission Lines

V. A. Soukhanovskii, D. W. Johnson, R. Kaita, A. L. Roquemore

May 1, 2007

Review of Sci. Instrum.

Disclaimer

Electron density measurements in the National Spherical Torus Experiment detached divertor region using Stark broadening of deuterium infrared Paschen emission lines

V. A. Soukhanovskii

Lawrence Livermore National Laboratory, Livermore, California

D. W. Johnson, R. Kaita, A. L. Roquemore

Princeton Plasma Physics Laboratory, Princeton, New Jersey

Abstract

Spatially resolved measurements of deuterium Balmer and Paschen line emission have been performed in the divertor region of the National Spherical Torus Experiment using a commercial 0.5 m Czerny-Turner spectrometer. While the Balmer emission lines, Balmer and Paschen continua in the ultraviolet and visible regions have been extensively used for tokamak divertor plasma temperature and density measurements, the diagnostic potential of infrared Paschen lines has been largely overlooked. We analyze Stark broadening of the lines corresponding to $2 - n$ and $3 - m$ transitions with principle quantum numbers $n = 7 - 12$ and $m = 10 - 12$ using recent Model Microfield Method calculations (C. Stehle and R. Hutcheon, Astron. Astrophys. Supl. Ser. 140, 93 (1999)). Densities in the range $(5 - 50) \times 10^{19}$ m^{-3} are obtained in the recombining inner divertor plasma in 2-6 MW NBI H-mode discharges. The measured Paschen line profiles show good sensitivity to Stark effects, and low sensitivity to instrumental and Doppler broadening. The lines are situated in the near-infrared wavelength domain, where optical signal extraction schemes for harsh nuclear environments are practically realizable, and where a recombining divertor plasma is optically thin. These properties make them an attractive recombining divertor density diagnostic for a burning plasma experiment. This work is supported by U.S. DoE under Contracts No. W-7405-Eng-48 and DE-AC02-76CH03073.

I. INTRODUCTION

Stark broadening of atomic hydrogen and deuterium high-n series emission lines, where n is a principle quantum number, has been used for spectroscopic measurements of plasma density in laboratory experiments, and evaluation of plasma conditions in stellar atmospheres [1]. The broadening is due to the linear Stark effect in a radiating oscillator (neutral emitter) caused by the electric microfield of charged perturbers - plasma electrons and ions. In magnetically confined fusion (MCF) plasma devices divertor heat flux reduction is achieved by volume momentum and energy dissipative processes. The process is known as divertor detachment and is often accompanied by plasma volume recombination. The three-body recombination process has been identified as a principle populating mechanism of the upper levels of the deuterium Balmer ($n_{lower} = 2$) and Paschen ($n_{lower} = 3$) series lines under the conditions of the recombining divertor plasma where T_e is low (0.5-1.5 eV) and n_e is high ($\leq 1 - 7 \times 10^{19}$ m^{-3}) [2]. We use the astrophysical notation for the series lines: for example, H10 is used for the Balmer $10 - 2$ transition, and P10 for the Paschen $10 - 3$ transition. The corresponding ultraviolet (UV) H6-H14 and near-infrared (NIR) P8-P14 lines have been observed in many divertor MCF experiments [3–6]. While the Stark-broadened Balmer lines, as well as the Balmer and Paschen continua emissions have been extensively used for diagnosing tokamak detached divertor plasma conditions, no application of the NIR Paschen lines has been reported. In this article we discuss electron density n_e measurements in the detached divertor plasma region of the National Spherical Torus Experiment (NSTX) using Stark broadening of the H7-H13 and P10-P13 lines. We demonstrate the density diagnostic utility of the Paschen lines by considering the spectroscopic measurement and analysis requirements and comparing them to the Balmer line results. We find that the Paschen NIR lines show good sensitivity to Stark effects in the range $n_e \geq 3 - 5 \times 10^{19}$ m^{-3}, and low sensitivity to instrumental and Doppler broadening. The P10 - P13 lines are essentially free from blending with impurity ion and molecular band emission lines. These properties make the measurements an attractive recombining divertor density diagnostic of a burning plasma, such as an ITER reference operating regime - an H-mode with a partially detached divertor. The use of NIR spectroscopy for a burning plasma experiment also appears to be advantageous in respect to the signal extraction requirements. Various spectroscopic signal extraction schemes based on reflective and transmissive optics such as windows, mirrors and

fibers, are presently being developed for the harsh nuclear environment. In a fusion reactor type device the elements of a diagnostic signal extraction line will be routinely exposed to high energy photon, neutron and particle fluxes. The degradation of reflective properties of metal mirrors is due to the material erosion and deposition. However, the degradation in the NIR range is not as severe as in the UV and visible ranges [7]. To address the transmission reduction problem in the intense gamma and neutron flux environments conventional optical fibers can be replaced by hollow optical fibers based on constructive interference on a layer of sub-wavelength holes surrounding a larger hollow core ([8] and references therein). The bandpass of the fibers is optimized for the visible and NIR light while the attenuation below 4500-5000 Å is high, making these fibers suitable for IR measurements in a burning plasma environment.

II. EXPERIMENT

The spectroscopic diagnostic arrangement is shown in Fig. 1. It comprised an imaging lens mounted on an upper NSTX Pyrex window port with a view of the lower divertor, a 50 m long quartz fiber bundle relay optics, and a commercial spectrometer. The imaging lens was a Nikon 85-mm $f/1.4$ model Nikkor NI8514DAF. The 32-fiber bundle included eight 1 mm core diameter fibers and twenty four 0.6 mm core diameter fibers, arranged to view, the outboard and inboard divertor regions, respectively. This layout provided a good spatial coverage of the strike point regions of the plasma shapes with both low and high triangularity and elongation as shown in Fig. 1. The focusing and spatial calibration of the fiber bundle - lens system were done *in-situ* by back-illuminating each fiber with a He-Ne laser. When back-illuminated, the fiber bundle - lens combination produced 1 cm diameter spots separated by 2 cm center-to-center distance in the inner divertor, and $1.5 - 2$ cm diameter spots separated by $4 - 5$ cm distance on the outboard divertor plate. Spot coordinates were measured with a computerized measuring arm with sub-mm precision in the vacuum vessel system of reference. For the present pilot measurements an Acton Research Model Spectro-Pro 500i 0.5 m $f/6.5$ Czerny-Turner spectrometer with three input fibers was used. The spectrometer was located in a radiation-shielded room 30 m away from the NSTX Test Cell. An *f*-number matching lens system imaged fiber ends on the spectrometer entrance slit.The spectrometer was equipped with 600, 1200, and 2400 l/mm gratings and the Princeton Instruments Model

Spec-10:100B spectroscopic charge-coupled device (CCD) 1340 × 100 pixel detector. The spectrometer instrumental function was measured using the mercury lamp lines at 3650, 4047, 8516, 9115, and 9216 Å. The instrumental function was described by a Gaussian profile with the full width at half-maximum (FWHM) of 1.13 Å in the UV region with the 1200 l/mm grating, and 2.30 Å in the NIR region with the 600 l/mm grating. The choice of gratings is a compromise between the spectral dispersion (resolution) and the spectral coverage in the UV and NIR regions, respectively. The photometric calibration of the spectrometer was done *in-situ* with the LabSphere URS-600 radiance standard placed inside the NSTX vacuum vessel. The sensitivity rapidly decreased in the UV region, apparently due to the attenuation in the lens and fibers. Because of the transmission cut-off at about 3500 Å second-order grating diffraction contribution was not an issue for the UV spectra. However, the efficiency of the 600 l/mm replica grating in the second order was found to be high, rendering the results of the NIR photometric calibration impractical, and the analysis of the P13-P15 lines difficult. An edge IR filter with a cut-off at 7200 Å was used to eliminate the second order diffraction contribution to the spectra. An *in-situ* photometric calibration with the edge filter would be preformed to back-calibrate these spectra. The NIR spectra presented in this article were recorded without the edge filter. The P10-P12 line profiles in these spectra were affected mostly through the background contribution.

III. METHOD, RESULTS AND DISCUSSION

A proper analysis of complex spectral features includes a rigorous collisional-radiative model for all deuterium free-bound and bound-bound transitions with ionization - recombination physics, molecular processes, radiative transfer and line shapes. It must also account for the plasma parameter distributions and the diagnostic viewing geometry. This has been accomplished with various degrees of completeness for the Balmer line emission recorded in MCF experiments [9–12]. In Stark broadening theoretical calculations, a number of authors use the impact theory for the electron component contribution to the hydrogen line profiles, and the quasi-static approximation for the ion component contribution. Progress has been made in recent years to generalize the theory to include ion dynamic contributions, as in the Model Microfield Method (MMM) calculations [13]. The MMM describe consistently both the line profile centers and the wings across a wide density range bridging the impact and

4

quasi-static treatments. Although the effect of ion dynamics is not as critical for the line profiles measured under the recombining (detached) divertor plasma conditions as it is for stellar atmosphere modeling, we use the most recent MMM calculations [13] in the NSTX spectra analysis.

While we are evaluating the analysis and modeling options for the NSTX experimental spectra, a reduced complexity analysis is used as outlined below. It addresses the experimental aspects of extracting pure Stark profiles for each line and accounting for the line blending and bremstrahlung background contributions. We note that opacity effects under the detached divertor conditions have been found insignificant for the intensity and profile analysis of the Balmer and Paschen lines (e.g. [10]). Shown in Fig. 2 are Balmer and Paschen line spectra emitted in the inner divertor region of 4-6 MW NBI heated NSTX plasmas. A total profile of each line can described by an integral convolution of Gaussian, Lorentzian and Voigt profiles resulting from several line broadening mechanisms [14]. For the NSTX divertor plasma parameters (magnetic field $B_{tot} \leq 0.1$ T, neutral density $n_d \leq 5 \times 10^{19}$ m^{-3}) the thermal and Stark broadening mechanisms are considered significant, whereas the natural broadening, Van der Waals broadening, and the broadening due to the Zeeman splitting are considered insignificant and neglected. Accordingly, the instrumental, thermal and Stark line profiles are considered in the total profile analysis: $\Gamma_{tot} = \Gamma_{instr} * \Gamma_{therm} * \Gamma_{Stark}$, where the convolution procedure (folding integral) is expressed by the symbol "$*$". A multi-peak function consisting of Voigt profiles for the deuterium lines and Gaussian profiles for impurity ion lines with a polynomial background is fitted to the measured spectra using a chi-square numerical fitting procedure. We use the numerical Levenberg-Marquardt least-square minimizer MPFIT [15] written in the IDL programming language. The fitting procedure works well for the deuterium lines with high signal-to-noise ratio, however it can be problematic for spectra with molecular line emission contributions. The BD and CD B-X molecular band emission can be quite prominent in the divertor attached phase and during the transition to the detached phase as shown in Fig. 2. The line profile analysis proceeds as follows. A Voigt profile by definition is an integral convolution of a Gaussian and a Lorentzian profiles. A number of numerical methods can be used to obtain a pure Stark profile from a Voigt profile fitted to experimental data. Since the Gaussian instrumental profile is measured, it would be possible to compute an integral convolution with a varying Lorentzian profile numerically until the sum of the weighted squared differences between the resulting Voigt profile and

5

the data is minimized. To avoid a direct numerical calculation of the Voigt integral for each line, however, we adopted a different approach. Our spectral line fitting procedure uses a fast and accurate approximation of the Voigt profile [16]. To obtain a pure Stark profile the following mathematical properties of the convolution integral can be used (for example, [14, 17]): a convolution of a Gaussian instrumental profile Γ_{instr} and a Gaussian thermal profile Γ_{therm} yields a Gaussian profile Γ_{i+th}, whereas a convolution of a Lorentzian profile describing the Stark broadening Γ_{Stark} and the Gaussian profile $\Gamma_{i_{th}}$ yields the Voigt profile Γ_{tot}. We further employ the property of a Fourier transform of the convolution integral: if $V = G * L$, then $f(V) = f(G) \times f(L)$, where f is an integral Fourier transform, and V, G and L are the Voigt, Gaussian and Lorentzian profiles, respectively. The deconvolution of the Gaussian and Lorentzian profiles is possible by taking an inverse Fourier transform of $f(V)/f(G)$. Thus a Stark full-width at half-maximum (FWHM) can extracted by fitting a Lorentzian profile to the obtained pure Stark profile. Such a rigorous deconvolution procedure may be necessary for the H7-H10 lines, where FWHM of the convolution of the instrumental and thermal 2 eV Gaussian profiles is about 1.7 Å. However, it does not have any impact on the NIR P10-P13 line analysis: the Gaussian FWHM is about 4 Å whereas the Voigt profile FWHM's are in the range of 10-30 Å. Shown in Fig. 3 is the electron density as a function of the Stark width for the H10 and the P10 lines compiled from the tabulated results of Ref. [13]. For comparison also shown are the representative 2 eV and 10 eV thermal line widths. It is evident that the Paschen line profile is subject to much less uncertainties associated with the instrumental and Doppler broadening mechanisms. The line width is sensitive to lower electron densities which are more relevant to the tokamak divertor.

Densities in the range $(5 - 50) \times 10^{19}$ m^{-3} have been measured in the NSTX inner divertor plasma region using the described method. The inner divertor leg is detached in NSTX throughout the operational space of NBI-heated discharges: $n_e \geq 2 - 3 \times 10^{13}$ cm^{-3} and $P_{NBI} \geq 0.8$ MW. Strong volume recombination is evident from the spatially resolved D$_\gamma$ and D$_\alpha$ profiles and high-n Balmer line spectroscopy [18–20]. The line emission takes place throughout the volume recombination zone, making the line-integrated spectroscopic measurement indicative of the highest n_e value in the detached divertor. Fig. 4 compares the inner divertor densities inferred from the H7-H11 and P10-P13 lines in similar 1 MA 6 MW NBI H-mode discharges. Divertor density time histories follow are slightly different

during the lower $\bar{n}_e$ phase, however they are essentially the same in the higher $\bar{n}_e$ phase. Shown in Fig. 5 is the time trace of the divertor density inferred from the P10-P11 lines in a high-performance 4 MW NBI H-mode plasma discharge. Despite the rise of the main plasma density throughout the discharge the inner divertor leg density remains nearly constant.

In summary, we are developing a multichannel spectroscopic diagnostic and the corresponding analysis for divertor electron density measurements using Stark broadened Balmer and Paschen emission lines originating from $n = 7 - 13$ levels. Our pilot measurements demonstrate a good density diagnostic potential of the Paschen lines for the recombining divertor-relevant density range. The Paschen line profile measurement has a number of advantages. It is undemanding to the spectrometer resolution because of the large Stark broadening, and it is situated in the NIR spectral region, where detectors, gratings, mirrors and relay optics have good sensitivity, reflection and transmission properties. Future work on NSTX will focus on comparison of the spectroscopic density measurements to divertor tile Langmuir probe measurements, an integrated spectral analysis of line shapes and intensities, and a design study of an imaging spectrometer which would take full advantage of the multi-channel fiber-optic system.

[1] H. R. Griem, Phys. Scripta **T83**, 142 (1999).

[2] D. Lumma, J. L. Terry, and B. Lipschultz, Physics of Plasmas **4**, 2555 (1997).

[3] J. L. Terry, B. Lipschultz, A. Y. Pigarov, S. I. Krasheninnikov, B. Labombard, D. Lumma, H. Ohkawa, D. Pappas, and M. Umansky, Phys. Plasmas **5**, 1759 (1998).

[4] B. Welch, H. Griem, J. Weaver, J. Brill, J. Terry, B. Lipschultz, D. Lumma, G. McCracken, S. Ferri, A. Calisti, R. Stamm, B. Talin, and R. Lee, AIP Conf. Proc. (USA) **386**, 113 (1997).

[5] A. Meigs, G. McCracken, C. Maggi, R. Monk, L. Horton, M. von Hellermann, M. Stamp, and P. Breger, in *Proc. 27th EPS Conf. on Contr. Fusion and Plasma Phys.* (Budapest, Hungary, 2000), Vol. ECA 24B, pp. 1264–1267.

[6] B. L. Welch, H. R. Griem, J. Terry, C. Kurz, B. LaBombard, B. Lipschultz, E. Marmar, and G. McCracken, Physics of Plasmas **2**, 4246 (1995).

[7] A. Litnovsky et al., J. Nuc. Mater., submitted (2006).

[8] D. Stutman, M. Finkenthal, G. Suliman, K. Tritz, L. Delgado-Aparicio, R. Kaita, D. Johnson, V. Soukhanovskii, and M. J. May, Rev. Sci. Instrum. **76**, 023505 (2005).

[9] M. Koubiti, H. Capes, L. Godbert-Mouret, Y. Marandet, A. Meigs, S. Loch, R. Stamm, and H. Summers, in *Spectral Line Shapes*, AIP Conf. Proc. (AIP, USA, 2002), No. 645 (1), pp. 67–73.

[10] H. A. Scott, A. S. Wan, D. E. Post, M. E. Rensink, and T. D. Rognlien, J. Nuc. Mater. **266-299**, 1247 (1999).

[11] A. Y. Pigarov, J. L. Terry, and B. Lipschultz, Plasma Phys. Control. Fusion **40**, 2055 (1998).

[12] H. P. Summers, W. J. Dickson, M. G. O'Mullane, N. R. Badnell, A. D. Whiteford, D. H. Brooks, J. Lang, S. D. Loch, and D. C. Griffin, Plasma Phys. Control. Fusion **48**, 263 (2006).

[13] C. Stehle and R. Hutcheon, Astron. Astrophys. Suppl. Ser. **140**, 93 (1999).

[14] D. F. Gray, *The Observation and Analysis of Stellar Photospheres* (Cambridge University Press, Cambridge ; New York, 1992).

[15] C. Markwardt, http://cow.physics.wisc.edu/∼craigm/idl/idl.html, 2006.

[16] J. Humlicek, J. Quant. Spectrosc. Radiat. Transfer **27**, 437 (1982).

[17] S. G. Rautian, Soviet Physics Uspekhi **66(1)**, 245 (1958).

[18] V. Soukhanovskii, R. Maingi, A. Roquemore, J. Boedo, C. Bush, R. Kaita, H. Kugel, B. LeBlanc, S. Paul, G. Porter, and N. Wolf, J. Nucl. Mater. **337-339**, 475 (2005).

[19] V. Soukhanovskii, A. Roquemore, C. Skinner, J. Menard, H. Kugel, D. Johnson, R. Maingi, S. Sabbagh, and F. Paoletti, Rev. Sci. Instrum. **74**, 2094 (2003).

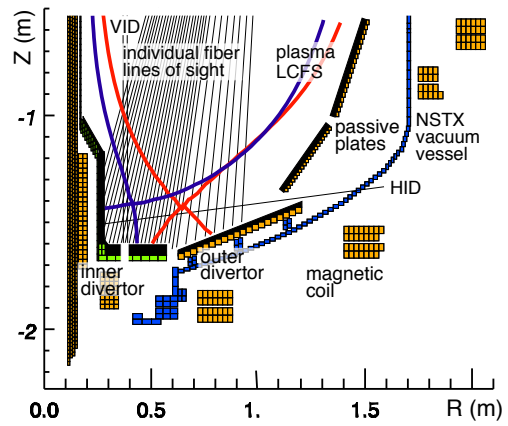[20] V. A. Soukhanovskii et al., J. Nuc. Mater., submitted (2006).

List of Figures

FIG. 1: Schematic of NSTX divertor multi-channel spectroscopy system consisting of 32 divertor lines of sight passing through the main plasma, and two local inner divertor lines of sight (labeled VID and HID). Actual spatially calibrated data are shown. Plasma last closed flux surfaces (LCFS) of low and high triangularity and elongation shapes are also shown.
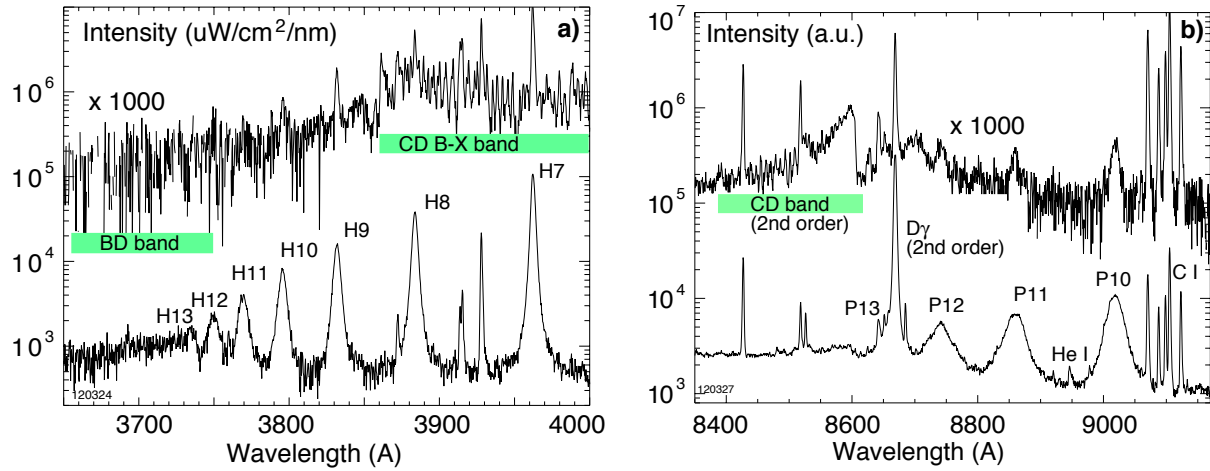
FIG. 2: Balmer (a) and Paschen (b) spectra measured in the NSTX detached divertor along the VID line of sight. The top spectra in (a) and (b) are obtained in the attached divertor phase, while the bottom spectra correspond to the detached phase.
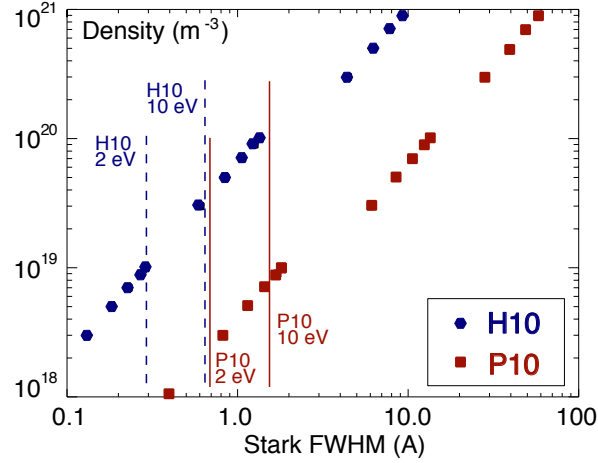
FIG. 3: Electron density as a function of Stark FWHM calculated from data in Ref. [13] for the H10 and P10 lines. Also shown are Doppler widths for $T_e = 2$ and 10 eV.
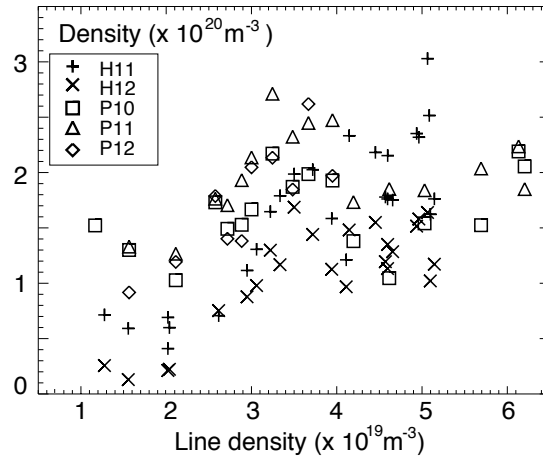

FIG. 4: Comparison of inner divertor density inferred from Balmer and Paschen lines in similar 4 MW NBI-heated plasmas as a function of main plasma line-averaged density. Error bars similar to those in Fig. 5 are not shown for clarity.
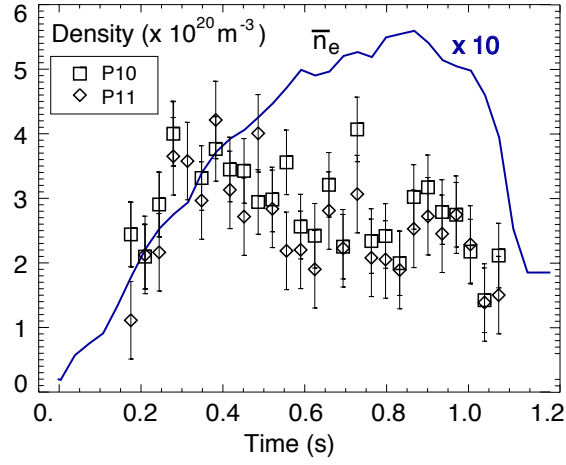
FIG. 5: Comparison of the detached divertor density inferred from the P10 and P11 lines